THE JOURNAL OF PHYSICAL CHEMISTRY Letters

Letter

pubs.acs.org/JPCL

Infrared Probes Based on Nitrile-Derivatized Prolines: Thermal Insulation Effect and Enhanced Dynamic Range

Kwang-Hee Park,[†] Jonggu Jeon,[†] Yumi Park,[†] Soyoung Lee,[†] Hyeok-Jun Kwon,[†] Cheonik Joo,[†] Sungnam Park,*[,†,‡] Hogyu Han,*[,†] and Minhaeng Cho*[,†,‡]

[†]Department of Chemistry, Korea University, Seoul 136-713, Korea

[‡]Multidimensional Spectroscopy Laboratory, Korea Basic Science Institute, Seoul 136-713, Korea

Supporting Information

ABSTRACT: Vibrational chromophores that are sensitive to local electrostatic environment are useful probes of structural variations of proteins on subnanosecond time scales, but their short vibrational lifetimes often limit their applicability. Here we explore a possibility to increase the lifetime of nitrile probes by introducing heavy atoms between the probe and protein side chains. Stereoisomers of thiocyanato- and selenocyanato-derivatized prolines, Pro-SCN and Pro-SeCN, are synthesized, and their CN stretch lifetimes in D_2O and chloroform are measured with polarization-controlled IR pump−probe spectroscopy. The measured lifetimes of 170−330 ps for Pro-SeCN are three to four times longer than those for Pro-SCN, indicating that selenium atom is more effective than sulfur atom in blocking the intramolecular vibrational relaxation pathways of the CN stretch mode. This is further confirmed by carrying out nonequilibrium molecular dynamics simulations of the vibrational relaxation processes. Given the crucial role of the proline residue in determining protein structures, we anticipate that the Pro-SeCN probe can be an excellent site-specific probe of changes in protein local environment.

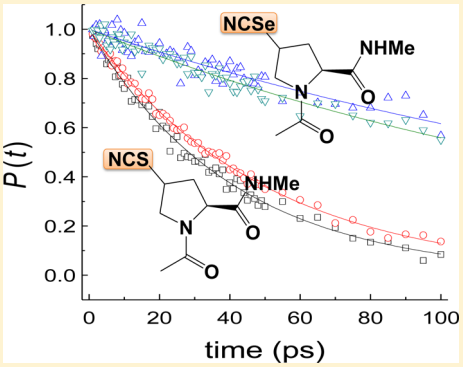

SECTION: Spectroscopy, Photochemistry, and Excited States

A variety of IR probes such as nitrile, thiocyanato, and azido groups and isotope-edited IR probes have been extensively used to measure local electric field and to monitor structural variations of proteins and nucleic acids because they can be site-specifically incorporated into biomolecules, and also their vibrational properties are highly sensitive to local electrostatic environment.[1−15] Various spectral features such as their IR band positions and bandwidths are affected by fluctuating solute−solvent intermolecular interaction, hydrophobic effect, hydrogen-bonding, and so on.[2,16−23]

In addition to their structural sensitivities, the site-specific IR probes should have sufficiently long vibrational lifetimes to be used for studying the protein dynamics occurring on time scales of hundreds of picoseconds. This is because the transient IR signals such as IR pump−probe and two-dimensional infrared (2DIR) signals of proteins in thermal equilibrium states can be measured only when the IR probes are on vibrationally excited states. In this regard, developments of new IR probes with long vibrational lifetimes are very important in vibrationally probing various structural dynamics of proteins occurring on hundreds of picoseconds or even longer time scales.

For studying local conformational changes of proteins, one of the target residues in various secondary and tertiary structure proteins is proline. It has a unique structure of five-membered pyrrolidine ring and plays a pivotal role in determining the global structures, functions, and dynamics of proteins.[20,24−28] In particular, the cis−trans isomerization of the peptidyl−prolyl bond is critically involved in the conformations and activities of peptides and proteins such as β-turn and β-hairpin.[29,30] In particular, 4-hydroxy proline derivative is one of the most important and naturally occurring proline derivatives found in structural proteins such as collagen.[31,32] The OH group in the 4-hydroxylproline can be readily replaced with either thiocyanato or selenocyanato group. With these site-specific IR probes, folding−unfolding dynamics of proline-containing peptides and proteins involving β-turn or β-hairpin structural motif might be readily studied.

In the present work, we stereoselectively synthesized (4*R*/4*S*)-thiocyanato (NCS-) and selenocyanato (NCSe-) proline derivatives (Figure 1A) and studied their vibrational relaxation dynamics in D_2O and $CHCl_3$, which represent the protic and aprotic solvents, respectively. Such proline derivatives can be potentially used as site-specific IR reporters in various proteins containing proline residues in the backbone. As shown in Figure 1, acetyl-4(*R*/*S*)-NCX-proline methyl amides are denoted as Pro-SCN(*R*), Pro-SCN(*S*), Pro-SeCN(*R*), and Pro-SeCN(*S*) according to the stereochemistry (*R*/*S*) at the fourth position of the pyrrolidine ring (or the C^{γ}-atom of proline) and the type of the bridge atom (S/Se) between the

Received: May 8, 2013
Accepted: June 6, 2013
Published: June 6, 2013

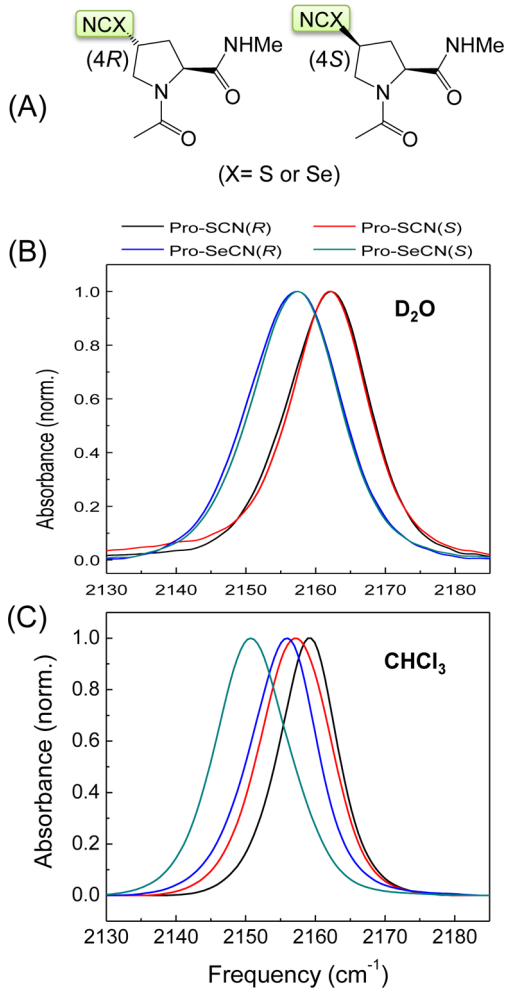

Figure 1. (A) Structures of acetyl-4(*R*/*S*)-NCX-proline methyl amides (for X = S or Se). Normalized nitrile stretch bands in the FTIR spectra of four proline derivatives (Pro-SCN(*R*), Pro-SCN(*S*), Pro-SeCN(*R*), and Pro-SeCN(*S*)) in (B) D_2O and (C) $CHCl_3$. The solvent background spectrum was properly subtracted.

CN group and the pyrrolindine ring. It turns out that these bridge atoms, S and Se, play an important role in blocking vibrational relaxation pathways of the CN stretch mode, as shown below.

Figure 1B,C displays the CN stretch bands in the FTIR spectra of four proline derivatives in D_2O and $CHCl_3$, respectively. For the sake of comparisons, the spectral features are also summarized in Table 1. In D_2O, the CN stretch band of thiocyanato group is ~5 cm^{-1} blue-shifted from that of selenocyanato group, and the different stereochemical configuration does not affect the peak positions and bandwidths appreciably. This indicates that the local environments around NCX groups in D_2O are very similar regardless of the stereochemistry of the substituted group because they strongly and preferentially interact with surrounding D_2O molecules and their intramolecular interactions with backbone peptides are less important. In contrast, the FTIR spectral features in $CHCl_3$ solutions shown in Figure 1C are quite different from those in D_2O. In particular, the peak positions depend sensitively on the stereochemistry of the vibrational chromophore, which indicates that the NCX groups in these four proline derivatives might have notably different local interactions in aprotic $CHCl_3$. The intramolecular interactions between NCX and backbone peptide bonds are likely to play dominant roles in determining the structure of the proline derivatives because the intermolecular interaction between the NCX group and $CHCl_3$ molecules is significantly weaker than that between the NCX group and D_2O molecules. This is consistent with our recent NMR and FTIR spectroscopic studies on 4-azidoproline.[33] We found that the backbone conformations of 4-azidoprolines in chloroform solutions are strongly affected by the intramolecular electrostatic or $n \rightarrow \pi^*$ interaction between (4*S*)-azido group and backbone peptide. It is believed that the (4*S*)-NCX groups in those prolines dissolved in $CHCl_3$ could form an intramolecular electrostatic interaction with *N*-methyl amide group.

Next, we studied the vibrational relaxation dynamics of the CN stretch modes in four proline derivatives by using polarization-controlled IR pump−probe (IR PP) spectroscopy, which involves a self-heterodyne detection of the third-order PP signal field.[34,35] Unlike the homodyne detection of the signal field, the heterodyne-detected signal is linearly proportional to the PP signal electric field so that its signal-to-noise ratio is greatly enhanced. Furthermore, in the case that there are multiple relaxation components contributing to the PP signal, they are additive so that the resulting signal can always be fit with multiple decaying functions, as will be demonstrated below.

Now, to selectively measure the vibrational population relaxation rates, a series of IR PP experiments were carried out in the magic-angle geometry, where the relative angle between the polarization directions of the pump and probe pulses was set to be 54.7°. The contribution of the orientational relaxation dynamics to the IR PP signal in the magic-angle configuration is suppressed because the measured signal $P(t)$ corresponds to the isotropic signal, that is

$$P(t) = \frac{S_{\parallel}(t) + 2S_{\perp}(t)}{3} \quad (1)$$

where $S_{\parallel}(t)$ and $S_{\perp}(t)$ are the parallel and perpendicular IR PP signals, respectively.

Figure 2A shows the dispersed isotropic IR PP signal measured with Pro-SCN(*S*) dissolved in D_2O. In IR PP experiments, the pump pulse initially promotes the molecules

Table 1. Spectral Features (Peak Frequency and fwhm (Full Width at Half-Maximum)) of the CN Stretch Bands of the Four Proline Derivatives in FTIR Spectra

	D_2O		$CHCl_3$	
	ω_{max} (cm^{-1})	fwhm (cm^{-1})	ω_{max} (cm^{-1})	fwhm (cm^{-1})
Pro-SCN(*R*)	2162	14.7	2159	10.4
Pro-SCN(*S*)	2162	14.4	2157	12.2
Pro-SeCN(*R*)	2157	16.0	2155	12.0
Pro-SeCN(*S*)	2157	15.5	2151	13.0

dx.doi.org/10.1021/jz400954r | *J. Phys. Chem. Lett.* 2013, 4, 2105−2110

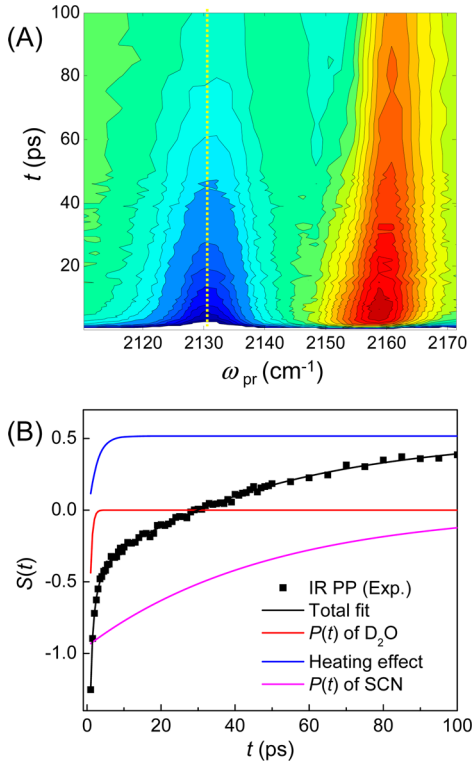

Figure 2. (A) Time- and frequency-resolved isotropic IR pump−probe signal, $P(t,\omega_{pr})$, measured with Pro-SCN(S) in D_2O. (B) Analysis of the isotropic IR PP signal measured at the $\upsilon = 1 \rightarrow 2$ transition (ω_{pr} = 2131 cm^{-1}, dashed line in panel A). To obtain the population decay of the CN stretch mode, $P(t, \omega_{pr}$= 2131 $cm^{-1})$ was fit by a model function. See the text and the Supporting Information for detailed discussions.

to vibrational excited states and the probe pulse is used to monitor the vibrational population relaxation back to their ground state as a function of the delay time t between the pump and probe pulses. The transmitted probe pulse is frequency-resolved to get the time- and frequency-resolved IR PP signal, $P(t,\omega_{pr})$. In Figure 2A, the high-frequency peak in red results from the ground-state bleach (GSB, $\upsilon = 0 \rightarrow 1$ transition) and stimulated emission (SE, $\upsilon = 0 \leftarrow 1$ transition, whereas the low-frequency peak in blue comes from the excited-state absorption (ESA, $\upsilon = 1 \rightarrow 2$ transition).[35] The GSB+SE contribution causes the transmission of the probe beam to increase giving the positive amplitude, whereas the ESA leads to the decrease in the transmission of the probe beam producing the negative signal. The dispersed isotropic IR PP signal decays as a result of the population relaxation.

In addition to the population decay component of the excited CN stretch mode, the isotropic PP signal shown in Figure 2A contains the contribution from the population decay of the excited OD stretch mode of solvent D_2O. It should be noted that the OD stretch mode of D_2O has a strong absorption at ~2510 cm^{-1} and the low-frequency tail of its IR band extends down to this spectral region. As a result, a small fraction of D_2O molecules are excited by the IR pump pulse as well and undergo population relaxations. The contribution of the OD stretch mode to the measured IR PP signal becomes more significant at higher frequencies. To reduce the contribution from the population relaxation of D_2O, we thus analyzed the isotropic IR PP signal at the $\upsilon = 1 \rightarrow 2$ transition frequency instead of the $\upsilon = 0 \rightarrow 1$ transition frequency of the CN stretch mode. The data points in Figure 2B are the isotropic IR PP signals at ω_{pr} = 2131 cm^{-1} ($\upsilon = 1 \rightarrow 2$), which is indicated as a white vertical line in Figure 2A. To extract the population relaxation constant of the CN stretch mode, we had to remove the vibrational relaxation of D_2O with a heating contribution from the total signal, as demonstrated in Figure 2B (see the blue line). For this, we used one of the standard procedures developed for analyzing the vibrational relaxation dynamics of water in liquid water. (See the Supporting Information for details and refs 36−38.) The measured isotropic IR PP signal was then successfully decomposed into three contributions: $P(t)$ of the CN stretch, $P(t)$ of the OD stretch, and the heating contribution resulting from the relaxation of excited OD stretch modes. Note that the vibrational population relaxation of the OD stretch mode is almost completed in just a few picoseconds (red line in Figure 2B) so that the subsequent heating contribution rises to a constant rapidly. In contrast, the population relaxation (green line in Figure 2B) of the CN stretch mode occurs on significantly longer time scales. Therefore, the isotropic IR PP signal at long times (>10 ps) is mainly determined by the population relaxation of the CN stretch mode.

The isotropic IR PP signals obtained from Pro-SCN(R), Pro-SeCN(R), and Pro-SeCN(S) in D_2O were also analyzed similarly. The resulting population relaxation of the CN stretch modes in the four proline derivatives in D_2O is shown in Figure 3A. For comparison, the isotropic IR PP signals measured with

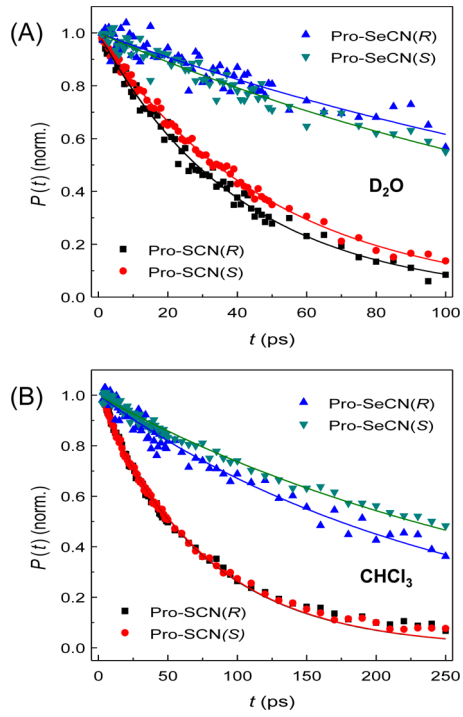

Figure 3. Population relaxation decays, $P(t)$, of the CN stretch modes in the four proline derivatives (A) in D_2O and (B) in $CHCl_3$.

Pro-SCN(R), Pro-SeCN(R), and Pro-SeCN(S) in $CHCl_3$, which do not contain any contributions from solvent $CHCl_3$, are also shown in Figure 3B. The corresponding vibrational lifetimes are summarized in Table 2. Overall, it turns out that the replacement of S with Se atom results in an increase in vibrational lifetime of the CN stretch mode by a factor of ~4.

dx.doi.org/10.1021/jz400954r | J. Phys. Chem. Lett. 2013, 4, 2105−2110

Table 2. Vibrational Lifetimes of the CN Stretch Modes in the Proline Derivatives

	D_2O		$CHCl_3$	
	ω_{pr} (cm^{-1})	T_1 (ps)	ω_{pr} (cm^{-1})	T_1 (ps)
Pro-SCN(R)	2131	45 ± 2	2159	75 ± 1
Pro-SCN(S)	2131	51 ± 2	2157	75 ± 1
Pro-SeCN(R)	2126	210 ± 60	2157	250 ± 6
Pro-SeCN(S)	2126	170 ± 24	2152	330 ± 5

In a polyatomic molecule, a large number of vibrational modes are anharmonically coupled and the potential energy surface is very complicated. Population relaxation of a given vibrational mode of a polyatomic molecule in solutions thus occurs through various intra- and intermolecular relaxation pathways. Here experimentally it was shown that the vibrational lifetimes of selenocyanato groups are much longer than those of thiocyanato groups in both solvents regardless of solvent's ability to form a hydrogen-bonding interaction with NCX group. As an example, let us consider the vibrational relaxation of Pro-SCN(R) and Pro-SeCN(R) in D_2O. Because the NCS and NCSe groups in these two compounds are exposed to neighboring D_2O molecules in a similar way, their intermolecular vibrational energy relaxation pathways to solvent degrees of freedom may not be so much different. In addition, their molecular structures would also be similar to each other in D_2O except the bridge atom (i.e., −S− or −Se−) between the CN group and the five-membered pyrrolidine ring. Nevertheless, the lifetime of Pro-SeCN(R) is found to be almost five times longer than that of Pro-SCN(R), which suggests that the bridge atom should play important roles in the intramolecular vibrational relaxation of the CN stretch mode. This observation is true for all corresponding pairs of thiocyanato- and selenocyanato-prolines in D_2O and $CHCl_3$. Here it should be mentioned that the vibrational lifetimes of the CN stretch modes of cyanophenol derivatives in methanol were observed to be just a few picoseconds.[39] In the case of cyanophenols, the CN stretch mode can be favorably coupled to delocalized modes of benzene ring because the CN group is directly attached to the benzene ring on the same plane. This linear linkage may provide effective intramolecular vibrational relaxation pathways, leading to relatively shorter lifetimes of the CN stretch modes. In contrast, the linkage between thiocyanato (or selenocyanato) group and pyrrolidine ring (i.e., NC−S−C^{γ} or NC−Se−C^{γ}) is not linear, and the CN stretch mode may not be effectively coupled to the pyrrolidine ring modes in proline derivatives as compared with cyanophenols or nitrile-derivatized tyrosine. In the cases of the thiocyanato- and selenocyanato-prolines, the intramolecular vibrational energy transfer of the CN stretch mode to the pyrrolidine ring modes is significantly hindered by the sulfur and selenium atoms, which behave like a thermal insulator such that the vibrational population relaxation of the CN stretch mode substantially slows down. The prolonged vibrational lifetimes of IR probes can clearly extend the measurement time range in time-resolved IR experiments because the temporal range of the signals measured in time-resolved IR spectroscopy is limited by the vibrational lifetimes of IR probes. In the present cases of the proline derivatives, the vibrational lifetime of NCSe group is much longer than that of NCS group.

The vibrational energy relaxation dynamics of the excited CN stretch mode in three proline derivatives (Pro-OCN(S), Pro-SCN(S), and Pro-SeCN(S)) were therefore studied with nonequilibrium molecular dynamics (NEMD) simulations employing a quantum mechanical/molecular mechanical (QM/MM) force field at the semiempirical PM3 level. The relaxation dynamics of the CN bond kinetic energy following a vibrational excitation at t = 0 for three proline derivatives are shown in Figure 4, and the exponential fit results are

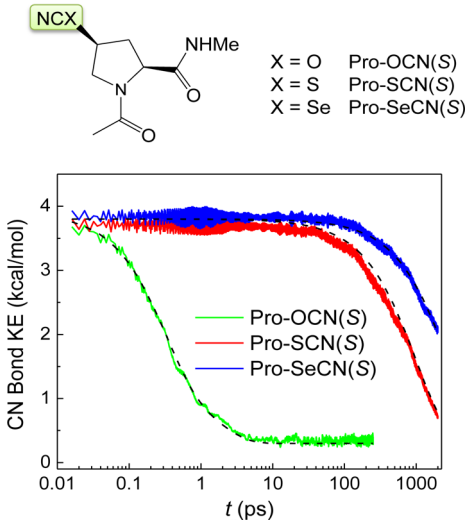

Figure 4. Kinetic energy decays of the CN bond of three proline derivatives (Pro-OCN(S), Pro-SCN(S), and Pro-SeCN(S)) following vibrational excitation at t = 0. Dashed lines are the exponential fits. See Table 3.

summarized in Table 3. The NEMD simulation appears to underestimate the vibrational energy relaxation rates of these proline derivatives when compared with the IR PP experimental results. However, the NEMD simulation results agree qualitatively well with our IR PP results in that the vibrational relaxation of Pro-SeCN(S) was estimated to be almost three times slower than that of Pro-SCN(S) in the NEMD simulation; note that the vibrational relaxation of Pro-SeCN(S) was measured to be roughly four times slower than that of Pro-SCN(S) in the present IR PP experiments. In addition, from the NEMD simulations, we found that the vibrational energy relaxation of Pro-OCN(S) is almost three orders of magnitude faster than those of Pro-SCN(S) and Pro-SeCN(S). Both IR pump−probe experiments and NEMD simulations indicate that the vibrational energy relaxation of the CN stretch mode becomes significantly slower as the bridge atom between the CN group and the pyrrolidine ring becomes heavier. This suggests that the heavier bridge atom behaves like a more efficient thermal insulator in the intramolecular vibrational relaxation of the CN stretch mode to the pyrrolidine ring modes in these proline derivatives.

In conclusion, we have studied the vibrational energy relaxation dynamics of the CN stretch mode in cyanato-, thiocyanato-, and selenocyanato-proline derivatives by IR pump−probe experiments and NEMD simulations. Both experimental and simulation results indicate that the vibrational energy relaxation of the CN stretch mode becomes slower in the order of cyanato-, thiocyanato-, and selenocyanato-proline derivatives. These observations are explained in terms of the insulating effects of the bridge atom between the CN group and pyrrolidine ring in proline derivatives, where a heavy bridge atom tends to prevent the intramolecular vibrational energy transfer from the localized CN stretch mode to the pyrrolidine

dx.doi.org/10.1021/jz400954r | J. Phys. Chem. Lett. 2013, 4, 2105−2110

Table 3. Exponential Fitting Results of the CN Bond Kinetic Energy Changes (Nonequilibrium Molecular Dynamics Simulation Results)

	K_1 (kcal/mol)	τ_1 (ps)	K_2 (kcal/mol)	τ_2 (ps)	K_∞ (kcal/mol)
Pro-OCN(*S*)	2.6	0.3	1.0	1.6	0.3
Pro-SCN(*S*)	3.5	1003			0.3
Pro-SeCN(*S*)	3.5	2800			0.3

*Fitting function has the general form $K(t) - K_\infty = \sum_n K_n \exp(-t/\tau_n)$.

ring modes, leading to an increase in vibrational lifetime of the CN stretch mode. The prolonged vibrational lifetime of an IR probe will allow us to extend temporal dynamic range measured in time-resolved IR experiments including IR pump−probe and 2DIR spectroscopy. The vibrational lifetimes of the CN stretch modes in selenocyanato-proline derivatives were found to be in the hundreds of picoseconds range. For real-time monitoring of the folding−unfolding dynamics, cis−trans isomerization, or local electric field change around the protein by using site-specific IR probes, the lifetime of IR probes should be sufficiently long. In this regard, the NCSe-group can be an excellent site-specific IR probe for studying protein dynamics of interest occurring in several hundred picoseconds, even in aqueous solutions.

■ ASSOCIATED CONTENT

Ⓢ Supporting Information

Detailed sample preparation, IR pump−probe measurements, nonequilibrium molecular dynamics simulation method, dispersed isotropic IR PP signals, and multicomponent fitting analysis results of the isotropic IR PP signals. This material is available free of charge via the Internet at http://pubs.acs.org.

■ AUTHOR INFORMATION

Corresponding Author

*E-mail: spark8@korea.ac.kr (S.P.); hogyuhan@korea.ac.kr (H.H.); mcho@korea.ac.kr (M.C.).

Notes

The authors declare no competing financial interest.

■ ACKNOWLEDGMENTS

This work was supported by the National Research Foundation of Korea (NRF) grants funded by the Korea government (MEST) (nos. 20090078897 and 20110020033) to M.C., the NRF grants (nos. 20100005020 and 20110002122) to S.P., the KETEP grant (no. 20104010100640) to S.P., and the NRF grant (no. 20100022070) to H.H..

■ REFERENCES

(1) Leeson, D. T.; Gai, F.; Rodriguez, H. M.; Gregoret, L. M.; Dyer, R. B. Protein Folding and Unfolding on a Complex Energy Landscape. *Proc. Natl. Acad. Sci. U.S.A.* **2000**, *6*, 2527−2532.

(2) Getahun, Z.; Huang, C. Y.; Wang, T.; DeLeon, B.; DeGrado, W. F.; Gai, F. Using Nitrile-Derivatized Amino Acids as Infrared Probes of Local Environment. *J. Am. Chem. Soc.* **2003**, *125*, 405−411.

(3) Suydam, I. T.; Snow, C. D.; Pande, V. S.; Boxer, S. G. Electric Fields at the Active Site of an Enzyme: Direct Comparison of Experiment with Theory. *Science* **2006**, *313*, 200−204.

(4) Fafarman, A. T.; Webb, L. J.; Chuang, J. I.; Boxer, S. G. Site-Specific Conversion of Cysteine Thiols into Thiocyanate Creates an IR Probe for Electric Fields in Proteins. *J. Am. Chem. Soc.* **2006**, *128*, 13356−13357.

(5) Decatur, S. M. Elucidation of Residue-Level Structure and Dynamics of Polypeptides via Isotope-Edited Infrared Spectroscopy. *Acc. Chem. Res.* **2006**, *39*, 169−175.

(6) Brewer, S. H.; Song, B.; Raleigh, D. P.; Dye, R. B. Residue Specific Resolution of Protein Folding Dynamics Using Isotope-Edited Infrared Temperature Jump Spectroscopy. *Biochemistry* **2007**, *46*, 3279−3285.

(7) Krummel, A. T.; Zanni, M. T. Evidence for Coupling between Nitrile Groups Using DNA Templates: A Promising New Method for Monitoring Structures with Infrared Spectroscopy. *J. Phys. Chem. B* **2008**, *112*, 1336−1338.

(8) Ye, S.; Zaitseva, E.; Caltabiano, G.; Schertler, G. F. X.; Sakmar, T. P.; Deupi, X.; Vogel, R. Tracking G-Protein-Coupled Receptor Activation Using Genetically Encoded Infrared Probes. *Nature* **2010**, *464*, 1386−1389.

(9) Taskent-Sezgin, H.; Chung, J.; Banerjee, P. S.; Nagarajan, S.; Dyer, R. B.; Carrico, I.; Raleigh, D. P. Azidohomoalanine: A Conformationally Sensitive IR Probe of Protein Folding, Protein Structure, and Electrostatics. *Angew. Chem., Int. Ed.* **2010**, *49*, 7473−7475.

(10) Choi, J.-H.; Raleigh, D.; Cho, M. Azido Homoalanine is a Useful Infrared Probe for Monitoring Local Electrostatistics and Side-Chain Solvation in Proteins. *J. Phys. Chem. Lett.* **2011**, *2*, 2158−2162.

(11) Tucker, M. J.; Gai, X. S.; Fenlon, E. E.; Brewer, S. H.; Hochstrasser, R. M. 2D IR Photon Echo of Azido-Probes for Biomolecular Dynamics. *Phys. Chem. Chem. Phys.* **2011**, *13*, 2237−2241.

(12) Bazewicz, C. G.; Lipkin, J. S.; Smith, E. E.; Liskov, M. T.; Brewer, S. H. Expanding the Utility of 4-Cyano-L-Phenylalanine as a Vibrational Reporter of Protein Environments. *J. Phys. Chem. B* **2012**, *116*, 10824−10831.

(13) Waegele, M. M.; Culick, R. M.; Gai, F. Site-Specific Spectroscopic Reporters of the Local Electric Field, Hydration, Structure, and Dynamics of Biomolecules. *J. Phys. Chem. Lett.* **2012**, *2*, 2598−2609.

(14) Bagchi, S.; Boxer, S. G.; Fayer, M. D.; Ribonuclease, S. Dynamics Measured Using a Nitrile Label with 2D IR Vibrational Echo Spectroscopy. *J. Phys. Chem. B* **2012**, *116*, 4034−4042.

(15) Middleton, C. T.; Marek, P.; Cao, P.; Chiu, C.-C.; Singh, S.; Woys, A. M.; De Pablo, J. J.; Raleigh, D. P.; Zanni, M. T. Two-Dimensional Infrared Spectroscopy Reveals the Complex Behaviour of an Amyloid Fibril Inhibitor. *Nat. Chem.* **2012**, *4*, 355−360.

(16) Hamm, P.; Lim, M.; Hochstrasser, R. M. Vibrational Energy Relaxation of the Cyanide Ion in Water. *J. Chem. Phys.* **1997**, *107*, 10523.

(17) Zhong, Q.; Baronavski, A. P.; Owrutsky, J. C. Vibrational Energy Relaxation of Aqueous Azide Ion Confined in Reverse Micelles. *J. Chem. Phys.* **2003**, *118*, 7074−7080.

(18) Bakker, H. J.; Kropman, M. F.; Omta, A. W.; Woutersen, S. Hydrogen-Bond Dynamics of Water in Ionic Solutions. *Phys. Scr.* **2004**, *69*, C14−C24.

(19) Fecko, C. J.; Loparo, J. J.; Roberts, S. T.; Tokmakoff, A. Local Hydrogen Bonding Dynamics and Collective Reorganization in Water: Ultrafast Infrared Spectroscopy of HOD/DO. *J. Chem. Phys.* **2005**, *122*, 054506.

(20) Kim, Y. S.; Hochstrasser, R. M. Chemical Exchange 2D IR of Hydrogen-Bond Making and Breaking. *Proc. Natl. Acad. Sci. U.S.A.* **2005**, *102*, 11185−11190.

(21) Maienschein-Cline, M. G.; Londergan, C. H. The CN Stretching Band of Aliphatic Thiocyanate Is Sensitive to Solvent Dynamics and Specific Solvation. *J. Phys. Chem. A* **2007**, *111*, 10020−10025.

(22) Zheng, J.; Fayer, M. D. Solute-Solvent Complex Kinetics and Thermodynamics Probed by 2D-IR Vibrational Echo Chemical Exchange Spectroscopy. *J. Phys. Chem. B* **2008**, *112*, 10221−10227.
(23) Lee, K.-K.; Park, K.-H.; Joo, C.; Kwon, H.-J.; Han, H.; Ha, J.-H.; Park, S.; Cho, M. Ultrafast Internal Rotational Dynamics of the Azido Group in (4S)-Azidoproline: Chemical Exchange 2DIR Spectroscopic Investigations. *Chem. Phys.* **2012**, *396*, 23−29.
(24) Jenkins, C. L.; Raines, R. T. Insights on the Conformational Stability of Collagen. *Nat. Prod. Rep.* **2002**, *19*, 49−59.
(25) Lummis, S. C. R.; Beene, D. L.; Lee, L. W.; Lester, H. A.; Broadhurst, R. W.; Dougherty, D. A. Cis-Trans Isomerization at a Proline Opens the Pore of a Neurotransmitter-Gated Ion Channel. *Nature* **2005**, *438*, 248−252.
(26) Lee, W. Y.; Sine, S. M. Principal Pathway Coupling Agonist Binding to Channel Gating in Nicotinic Receptors. *Nature* **2005**, *438*, 243−247.
(27) Brodsky, B.; Persikov, A. V. Molecular Structure of the Collagen Triple Helix. *Adv. Protein Chem.* **2005**, *70*, 301−339.
(28) Pastorino, L.; Sun, A.; Lu, P.-J.; Zhou, X. Z.; Balastik, M.; Finn, G.; Wulf, G.; Lim, J.; Li, S.-H.; Li, X.; Xia, W.; Nicholson, L. K.; Lu, K. P. The Prolyl Isomerase Pin1 Regulates Amyloid Precursor Protein Processing and Amyloid-beta Production. *Nature* **2006**, *440*, 528−534.
(29) Wedemeyer, W. J.; Welker, E.; Scheraga, H. A. Proline Cis-Trans Isomerization and Protein Folding. *Biochemistry* **2002**, *41*, 14637−14644.
(30) Lu, K. P.; Finn, G.; Lee, T. H.; Nicholson, L. K. Prolyl Cis-Trans Isomerization as a Molecular Timer. *Nat. Chem. Biol.* **2007**, *3*, 619−629.
(31) Hinderaker, M. P.; Raines, R. T. An Electronic Effect on Protein Structure. *Protein Sci.* **2003**, *12*, 1188−1194.
(32) Bartlett, G. J.; Choudhary, A.; Raines, R. T.; Woolfson, D. N. n → π^* Interactions in Proteins. *Nat. Chem. Biol.* **2010**, *6*, 615−620.
(33) Lee, K.-K.; Park, K.-H.; Joo, C.; Kwon, H.-J.; Jeon, J.; Jung, H.-I.; Park, S.; Han, H.; Cho, M. Infrared Probing of 4-Azidoproline Conformations Modulated by Azido Group Configurations. *J. Phys. Chem. B* **2012**, *116*, 5097−5110.
(34) Mukamel, S. *Principles of Nonlinear Optical Spectroscopy*; Oxford University Press: Oxford, U.K., 1995.
(35) Cho, M. *Two-Dimensional Optical Spectroscopy*; CRC Press: Boca Raton, FL, 2009.
(36) Steinel, T.; Asbury, J. B.; Zheng, J. R.; Fayer, M. D. Watching Hydrogen Bonds Break: A Transient Absorption Study of Water. *J. Phys. Chem. A* **2004**, *108*, 10957−10964.
(37) Piletic, I. R.; Moilanen, D. E.; Spry, D. B.; Levinger, N. E.; Fayer, M. D. Testing the Core/shell Model of Nanoconfined Water in Reverse Micelles Using Linear and Nonlinear IR Spectroscopy. *J. Phys. Chem. A* **2006**, *110*, 4985−4999.
(38) Rezus, Y. L. A.; Bakker, H. J. Orientational Dynamics of Isotopically Diluted H_2O and D_2O. *J. Chem. Phys.* **2006**, *125*, 144512.
(39) Lee, K.-K.; Park, K.-H.; Choi, J.-H.; Ha, J.-H.; Jeon, S.-J.; Cho, M. Ultrafast Vibrational Spectroscopy of Cyanophenols. *J. Phys. Chem. A* **2010**, *114*, 2757−2767.

Supporting information

Infrared Probes Based on Nitrile-Derivatized Prolines: Thermal Insulation Effect and Enhanced Dynamic Range

Kwang-Hee Park[1], Jonggu Jeon[1], Yumi Park[1], Soyoung Lee[1], Hyeok-Jun Kwon[1], Cheonik Joo[1], Sungnam Park[1,2*], Hogyu Han[1*], and Minhaeng Cho[1,2*]

[1]*Department of Chemistry, Korea University, Seoul 136-713, Korea*
[2]*Multidimensional Spectroscopy Laboratory, Korea Basic Science Institute, Seoul 136-713, Korea*

Contents

1. Experimental methods

***Sample preparation*:** Four proline derivatives (Pro-SCN(*R*), Pro-SCN(*S*), Pro-SeCN(*R*), and Pro-SeCN(*S*)) used in our experiments were synthesized. It should be noted that, even though Pro-OCN(*S*) was also investigated by carrying out nonequilibrium molecular dynamics simulations, we were not able to synthesize cyanato-derivatized prolines (Pro-OCN(*R*) and Pro-OCN(*S*)) due to their chemical instabilities during organic synthesis. Deuterium oxide (D_2O, 99.99%) and chloroform ($CHCl_3$, HPLC grade) were purchased from Sigma-Aldrich and used as received. The sample solutions were prepared by directly dissolving the proline derivatives in D_2O and $CHCl_3$. The concentrations of Pro-SCN(*R*) and Pro-SCN(*S*) were ~0.59 M in D_2O and ~0.29 M in $CHCl_3$, respectively. The concentrations of Pro-SeCN(*R*) and Pro-SeCN(S) were ~0.73 M in D_2O and ~0.36 M in $CHCl_3$. The sample solutions were housed in a homemade IR cell with two 3 mm CaF_2 windows. The path lengths of the IR cell was fixed with a 6 and 100 μm thick Teflon spacer (Harrick Scientific Products Inc.) for D_2O and $CHCl_3$ solutions, respectively. FTIR spectra of all sample solutions were collected by using the JASCO FTIR spectrometer (FT/IR-4100) with 2 cm^{-1} resolution.

***IR pump-probe measurement*:** Our IR pump-probe experimental setup was described elsewhere.[1-2] Briefly, mid-IR pulse centered at 2150 cm^{-1} (fwhm=250 cm^{-1}) with its energy of ~1.0 nJ was generated from our femtosecond laser systems and its chirp was properly compensated producing a transform-limited pulse at the sample position. The mid-IR beam was split by a ZnSe beamsplitter into the pump and probe beams with the intensity ratio of 2:1. The time delay between the pump and probe pulse was controlled by a motorized linear translational stage. The pump beam was vertically polarized and the polarization of the probe beam was rotated by 54.7° with respect to the polarization direction of the pump beam. By

using this magic-angle polarization geometry, isotropic IR PP signal was directly measured. The pump and probe pulses were focused onto the sample. The probe beam was collimated after the sample and dispersed through the monochromator onto a 64-element MCT (Mercury-Cadmium-Telluride) array detector where the probe beam was frequency-resolved. For a given delay time t, IR PP signal was measured by $S(t) = [T_{\text{pump-on}} - T_{\text{pump-off}}](t)/T_{\text{pump-off}} = \Delta T(t)/T$, where T was the transmission of the probe beam through the sample.[3]

***Nonequilibrium molecular dynamics simulation*:** The NEMD simulations were performed on isolated Pro-OCN(*S*), Pro-SCN(*S*), and Pro-SeCN(*S*) with the AMBER 9 package.[4-5] These proline derivatives were described with the semiempirical PM3 potential and an MM correction term was added to the peptide dihedral interactions. Each system was first equilibrated for 1 ns at 298 K. From the subsequent 2 ns trajectory under the same condition, 100 configurations were saved at equal intervals. To mimic the vibrational excitation of the CN bond, the CN bond was treated as a classical harmonic oscillator and the excitation is assumed to induce random and instantaneous changes to the coordinate and momentum of the local CN stretch mode so that its energy increases by $\hbar\omega$ (= 2200 cm^{-1} = 6.29 kcal/mol).[6]

The corresponding perturbations were applied to the nitrile C and N atomic positions and velocities in each of the 100 states selected above from the canonical ensemble. Starting from these initial states, the 100 independent NEMD trajectories were propagated for up to 2 ns under the microcanonical condition. The CN bond kinetic energy was calculated from the atomic velocities as $k_{\text{CN}} = \mu_{\text{CN}} \left| \mathbf{v}_{\text{N}} - \mathbf{v}_{\text{C}} \right|^2 / 2$ by average over the 100 samples of the nonequilibrium ensemble (μ_{CN}: reduced mass of CN unit). Details of the computational method can be found in Ref. 5.

2. Analysis of the isotropic IR PP signal[7-9]

The isotropic IR PP signal, $S(t)$, is fitted to the following equation,

$$S(t) = A_1 \exp(-t / T_{XCN}) + A_2 S_{D_2O}(t) \quad \text{(S1)}$$

where the first term corresponds to the population relaxation of the CN stretch mode and $S_{D_2O}(t)$ represents the population decay of OD stretch mode including a heating contribution. The vibrational relaxation dynamics of water were well studied before and were fitted to

$$S_{D_2O}(t) = \exp(-k_1 t) + \frac{\alpha}{k_1 + k_2}\left[k_1\left(1 - \exp(-k_2 t)\right) + k_2\left(-1 + \exp(-k_1 t)\right)\right] \quad \text{(S2)}$$

where k_1 is the rate constant associated with energy transfer from the CN excited state to the intermediate state and k_2 is the energy transfer rate constant from the intermediate state to heated states. Eq. (S2) has been used as one of the standard procedures for analyzing the vibrational relaxation dynamics of water in liquid water. The fitting parameters are summarized in Table S1.

SUPPORTING REFERENCES

(1) Lee, K.-K.; Park, K.-H.; Choi, J.-H.; Ha, J.-H.; Jeon, S.-J.; Cho, M. Ultrafast Vibrational Spectroscopy of Cyanophenols. *J. Phys. Chem. A* **2010**, *114*, 2757-2767.

(2) Kim, H.; Park, S.; Cho, M. Rotational Dynamics of Thiocyanate Ions in Highly Concentrated Aqueous Solutions. *Phys. Chem. Chem. Phys.* **2012**, *14*, 6233-6240.

(3) Son, H.; Kwon, Y.; Kim, J.; Park, S. Rotational Dynamics of Metal Azide Ion Pairs in Dimethylsulfoxide Solutions. *J. Phys. Chem. B* **2013**, *117*, 2748−2756.

(4) Case, D. A.; Darden, T.; Cheatham III, T. E.; Simmerling, C.; Wang, J.; Duke, R. E.; Luo, R.; Merz, K. M.; Pearlman, D. A.; Crowley, M. *et al. AMBER 9*, University of California: San Francisco, U.S.A., **2006**.

(5) Jeon, J.; Cho, M. Redistribution of Carbonyl Stretch Mode Energy in Isolated and Solvated N-methylacetamide: Kinetic Energy Spectral Density Analyses. *J. Chem. Phys.* **2011**, *135*, 214504.

(6) Nguyen, P. H.; Stock, G. Nonequilibrium Molecular-dynamics Study of the Vibrational Energy Relaxation of Peptides in Water. *J. Chem. Phys.* **2003**, *119*, 11350.

(7) Steinel, T.; Asbury, J. B.; Zheng, J. R.; Fayer, M. D. Watching Hydrogen Bonds Break: A Transient Absorption Study of Water. *J. Phys. Chem. A* **2004**, *108*, 10957-10964.

(8) Rezus, Y. L. A.; Bakker, H. J. Orientational Dynamics of Isotopically Diluted H_2O and D_2O. *J. Chem. Phys.* **2006**, *125*, 144512.

(9) Piletic, I. R.; Moilanen, D. E.; Spry, D. B.; Levinger, N. E.; Fayer, M. D. Testing the Core/shell Model of Nanoconfined Water in Reverse Micelles Using Linear and Nonlinear IR Spectroscopy. *J. Phys. Chem. A* **2006**, *110*, 4985-4999.

Table S1. Fitting parameters of isotropic IR PP signals of acetyl-4(*R/S*)-NCX-prolines dissolved in D_2O.

	A_1	A_2	α	k_1	k_2	T_{XCN}
Pro-SCN(*R*)	-0.87±0.02	-5.28±2.00	-0.23±0.11	2.61±0.35	0.61±0.05	40.8±2.35
Pro-SCN(*S*)	-0.76±0.01	-2.38±0.38	-0.29±0.05	1.92±0.15	0.48±0.03	49.0±2.25
Pro-SeCN(*R*)	-0.50±0.11	-7.53±2.50	-0.10±0.03	2.48±0.41	0.44±0.06	206.5±58.8
Pro-SeCN(*S*)	-0.64±0.07	-7.87±3.76	-0.08±0.03	2.83±0.54	0.34±0.04	171.6±24.3

SUPPORTING FIGURES

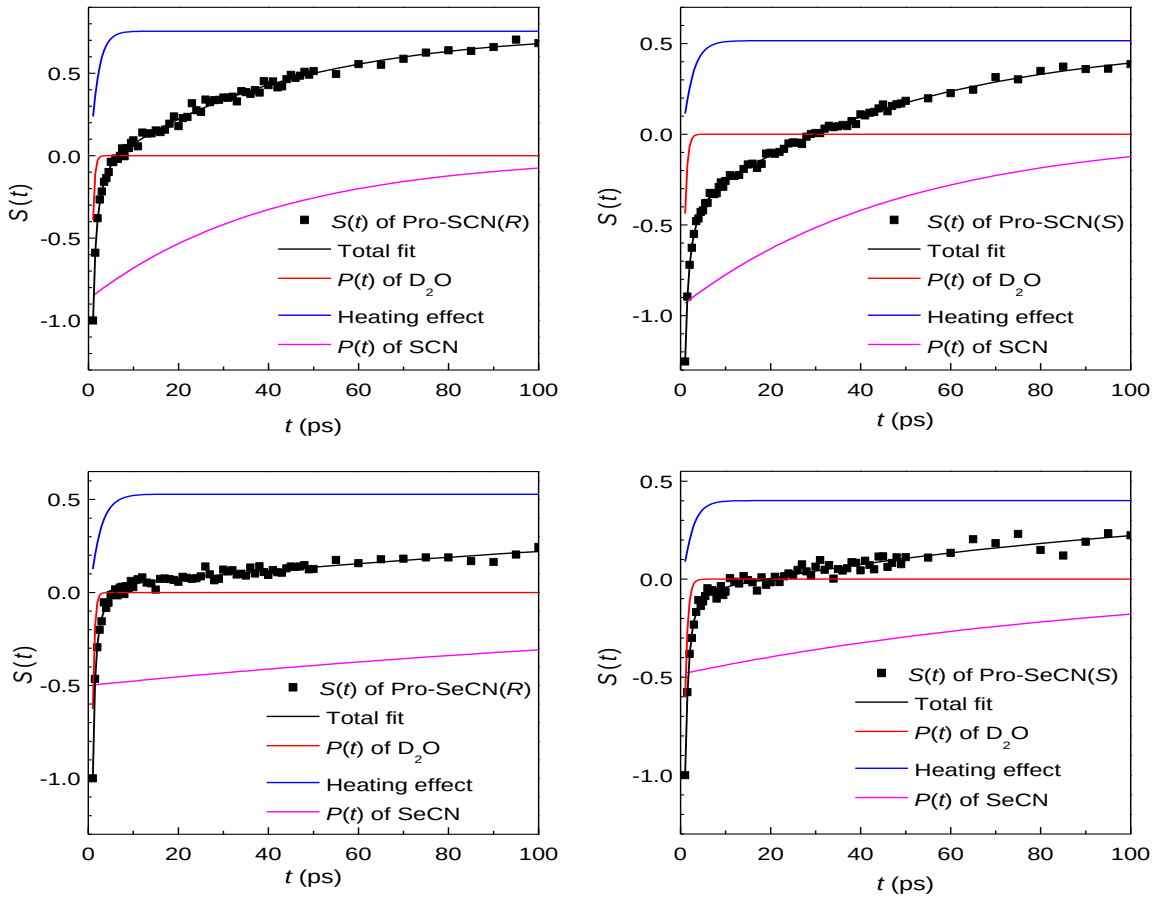

Figure S1. Decomposition of isotropic IR PP signals of acetyl-4(*R/S*)-NCX-prolines dissolved in D_2O. ($P(t)$ of CN stretch mode, $P(t)$ of D_2O, and heating contribution)

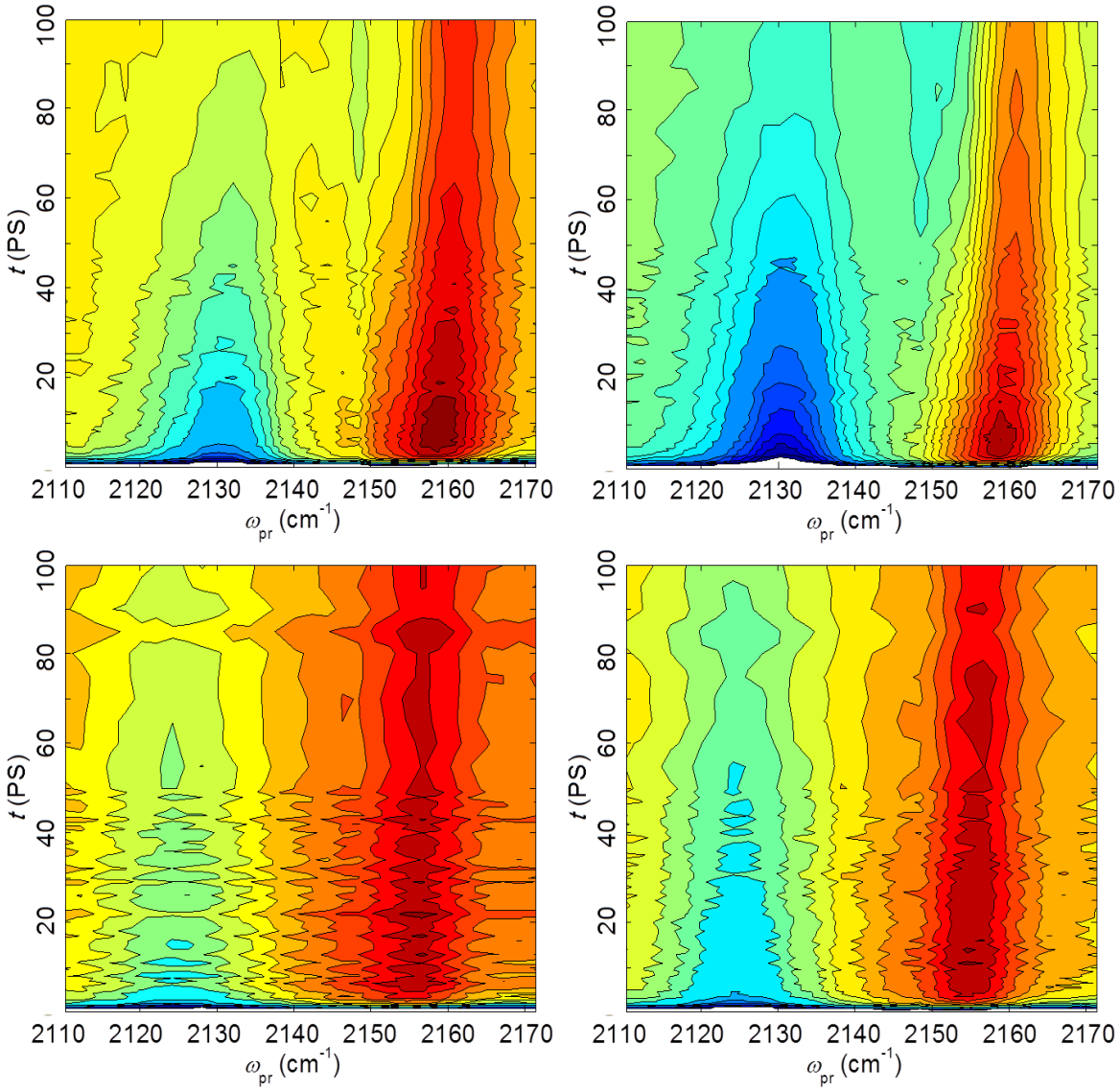

Figure S2. Dispersed isotropic IR PP signals of acetyl-4(*R/S*)-NCX-prolines dissolved in D_2O. (A) Pro-SCN(*R*), (B) Pro-SCN(*S*), (C) Pro-SeCN(*R*), and (D) Pro-SeCN(*S*).

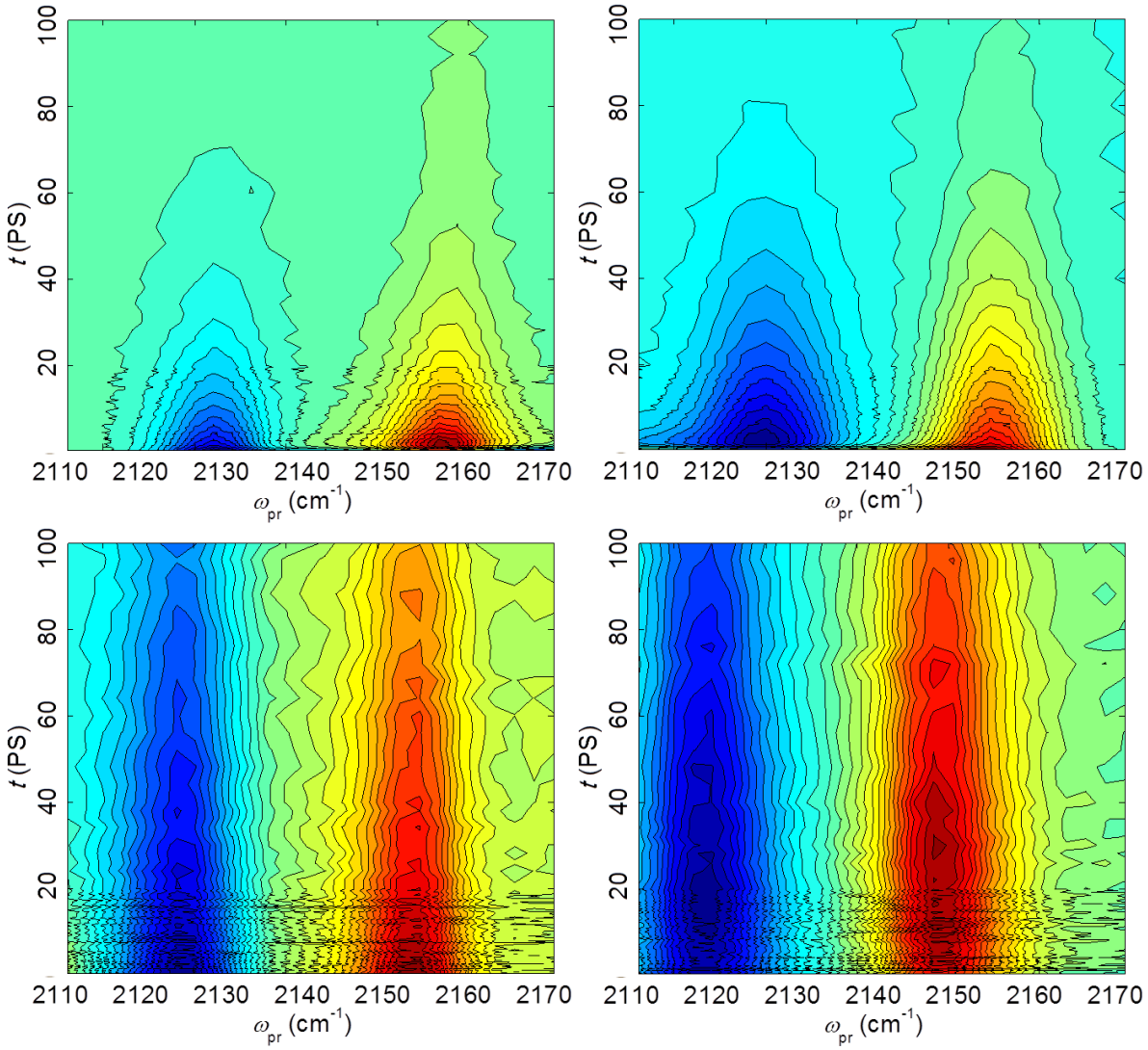

Figure S3. Dispersed isotropic IR PP signals of acetyl-4(*R/S*)-NCX-prolines dissolved in $CHCl_3$. (A) Pro-SCN(*R*), (B) Pro-SCN(*S*), (C) Pro-SeCN(*R*), and (D) Pro-SeCN(*S*).